

A Proposal of Nonlinear Formulation of Cell Method for Thermo-Elastostatic Problems

C. Delprete¹ F. Freschi², M. Repetto² and C. Rosso¹

Abstract: The growing necessity of accuracy in analyzing engineering problems requires more detailed and sophisticated models. Those models can include multiphysics interactions, that, sometimes, are highly nonlinear and the application of the superposition principle is then not possible. The cell method can be suitably used to study nonlinear multiphysics problems, because its theoretical framework for the physical laws is intrinsically multiphysics. In this way it is possible to take into account the mutual effects between different physics. Within the cell method framework, the coupling terms can be directly formulated in terms of the global variables used for the solution of the elementary problems. In this way it is possible to solve the coupled problem in a single solver run. In this paper a nonlinear procedure for elastostatic analysis with cell method is developed and the Fixed Point technique is applied to a 1D two-node cell and to a 3D four-node tetrahedral cell. The procedure is numerically and experimentally validated. After the theoretical part, a nonlinear thermo-mechanical analysis of an exhaust manifold is presented as case-study.

Keywords: cell method, nonlinear elastostatics, exhaust manifold, multiphysics

1 Introduction

The study of coupled nonlinear phenomena is increasingly becoming topical. In order to obtain more accurate results, closer to measurements, the superposition, often adopted in multiphysics analyses, can have some limitations. For reaching the goal, a naturally born multiphysics approach can be used.

Generally the analysis of a multiphysics system with commercial finite element (FE) softwares require the definition of different models, each dedicated to one

¹ Dipartimento di Ingegneria Meccanica e Aerospaziale, Politecnico di Torino, corso Duca degli Abruzzi, 24, 10129 Torino.

² Dipartimento Energia, Politecnico di Torino, corso Duca degli Abruzzi, 24, 10129 Torino.

specific physics; the results of one model are then used as input for the other models. For example, during the thermo-structural analysis of an automotive exhaust manifold, two models must be created: one for the thermal and one for the mechanical problem [Mamiya, Masuda, and Noda (2002); Su, Zubeck, Lasecki, Jr., Tang, Sehitoglu, and Allison (2002); Hazime, Dropps, Anderson, and Ali (2003); Constantinescu, Charkaluk, Lederer, and Verger (2004); Delprete and Rosso (2005); Wohrmann, Seifert, Willeke, and Hartmann (2006)]. The results of the thermal model are the inputs, together with the mechanical boundary conditions, for the mechanical model. Two models, two different sets of boundary conditions and two runs are then required for the solution of the whole problem. The cell method (CM) [Tonti (2001); Tonti and Zarantonello (2009); Cosmi (2001, 2005); Alotto, Freschi, Repetto, and Rosso (2013); Ferretti (2013a)] is a numerical technique suitable for the implementation of coupled multiphysics [Delprete, Freschi, Repetto, and Rosso (2010); Alotto, Freschi, and Repetto (2010); Moro, Alotto, Freschi, and Guarnieri (2012); Ferretti (2013b)] allowing a coupled simulation of the different physical phenomena, taking into account the mutual effects between the physical entities. The elastostatic formulation with the CM is currently not able to take into account nonlinear effects.

This paper proposes an extension of the CM for elastostatics with nonlinear materials. Many numerical techniques can be used to study nonlinear problems. In section 2 a brief overview of these methods is reported. For the CM, the authors suggest the use of the fixed point nonlinear iterative method [Chiampi, Chiarabaglio, and Repetto (1994)]. This choice has been adopted because the fixed point method presents some of computational advantages with respect to the other methods.

Details of the implementation of the fixed point technique within the CM framework are discussed in section 3. The proposed technique is then validated in section 4 and applied to the study of an exhaust manifold for automotive applications in section 5.

2 Overview of methods for the solution of nonlinear equations

A generic nonlinear problem can be mathematically expressed as [Zienkiewicz and Taylor (2000)]:

$$\mathbf{K}(\mathbf{a})\mathbf{a} = \mathbf{f} \quad (1)$$

An iterative scheme for solving Eq. (1) is made by a set of rules that, starting from a trial configuration, update the solution until a convergence criterion is satisfied. The simplest iterative technique proceeds by successively solving Eq. (1) where the

stiffness matrix is updated at each iteration with the new estimate of the solution:

$$\mathbf{K}(\mathbf{a}^{(i)})\mathbf{a}^{(i+1)} = \mathbf{f} \quad (2)$$

This method is not always stable and can be slow in convergence. For this reason is not used in commercial softwares. In the next sections other more common methods are described.

2.1 The Newton-Raphson technique

Re-formulating Eq. (1) as:

$$\Psi(\mathbf{a}) = \mathbf{K}(\mathbf{a})\mathbf{a} - \mathbf{f} = 0 \quad (3)$$

the difference function Ψ can be expanded by the truncated Taylors' series:

$$\Psi(\mathbf{a}^{(i+1)}) = \Psi(\mathbf{a}^{(i)}) + \frac{\partial \Psi_1}{\partial a_1} \Delta a_1^{(i)} + \frac{\partial \Psi_1}{\partial a_2} \Delta a_2^{(i)} + \dots + \frac{\partial \Psi_2}{\partial a_1} \Delta a_1^{(i)} + \frac{\partial \Psi_2}{\partial a_2} \Delta a_2^{(i)} + \dots \approx 0 \quad (4)$$

or, in matrix form

$$\Psi(\mathbf{a}^{(i)}) + \mathbf{J}(\mathbf{a}^{(i)})\Delta\mathbf{a}^{(i)} = 0 \quad \rightarrow \quad \mathbf{J}(\mathbf{a}^{(i)})\Delta\mathbf{a}^{(i)} = -\Psi(\mathbf{a}^{(i)}) \quad (5)$$

The system Eq. (5) is solved with respect to the vector of error values $\Delta a_1^{(i)}$ then, the improved solution $\mathbf{a}^{(i+1)}$ can be written as

$$\mathbf{a}^{(i+1)} = \mathbf{a}^{(i)} + \Delta\mathbf{a}^{(i)} \quad (6)$$

As far as the elastostatic problem is concerned, the Newton-Raphson technique is usually coupled with the incremental approach, where the external forces at the right-hand-side are progressively incremented from zero to their final value during the nonlinear iterations.

The Newton-Raphson technique has a quadratic convergence when a good starting solution is provided (for more detail see [Zienkiewicz and Taylor (2000)]), but it presents some limitations:

- the Jacobian matrix has to be computed at each iteration step;
- if a direct solution method is used, the Jacobian matrix has to be factorized at every step to solve Eq. (5);
- the Jacobian matrix can be ill-conditioned and can create numerical problem in the solution.

2.2 The modified Newton-Raphson technique

The method is based on the same algorithm of the classical Newton-Raphson, but the Jacobian matrix \mathbf{J} is estimated once and maintained constant at each iteration

$$\mathbf{J}^{(i)} = \mathbf{J}^{(0)} \tag{7}$$

Different approaches for the approximation of the Jacobian matrix can be used: the stiffness matrix can be chosen equal to the first iteration matrix or can be updated after several iterations. The convergence rate is no more quadratic, but some drawbacks of the standard Newton-Raphson method are removed.

2.3 The secant method

The procedure tries to combine the advantages of the standard and the modified Newton-Raphson methods [Zienkiewicz and Taylor (2000)]. At each step, the generic jk entry of the Jacobian matrix is estimated on the basis of the previous steps:

$$\{\mathbf{J}^{(i)}\}_{jk} = \frac{\{\Psi^{(i)}\}_j - \{\Psi^{(i-1)}\}_j}{\{\mathbf{a}^{(i)}\}_k - \{\mathbf{a}^{(i-1)}\}_k} \tag{8}$$

The computation of Eq. (8) could be difficult not unique: in fact many matrices can satisfy the initial problem and for this reason many starting alternative matrices are used in the practice.

2.4 The fixed point method

The problem Eq. (1) can be linearized, as described in Chiampi, Chiarabaglio, and Repetto (1994), computing the stiffness matrix for a suitable value of the material constant as:

$$\mathbf{K}_{fp}\mathbf{a} = \mathbf{f} - \mathbf{R} \tag{9}$$

\mathbf{K}_{fp} is the linearized stiffness matrix computed considering the material linear with a constant characteristic that has to be chosen in order to guarantee convergence. The vector \mathbf{R} is the nonlinear residual that is iteratively updated:

$$\mathbf{R}^{(0)} = \mathbf{0}, \quad \mathbf{R}^{(i+1)} = \mathbf{f} - \mathbf{K}(\mathbf{a}^{(i)})\mathbf{a}^{(i)} \tag{10}$$

Following the theoretical treatment proposed in [Chiampi, Chiarabaglio, and Repetto (1994)], the linearized value of the material characteristic which ensure the convergence is bounded between the minimum and maximum slope of the nonlinear characteristic. A specified tolerance on variation of the residual between two successive iterations is chosen as a convergence criterion.

With this method the stiffness matrix is estimated once and then it is used at each step. Only the right-hand-side of the equation is updated during the iterative process. For this reason, the fixed point method can be easily applied in combination with direct solvers, because the stiffness matrix is factorized once when the process starts, and for each iteration the residual update and the forward/backward substitutions are the only required operations.

3 Nonlinear formulation of the elastostatic problem with the CM and the fixed point technique

In this section the 1D and 3D analysis are analyzed. The former is considered because the only one stress (and strain) direction is present, simplifying the formulation. In the second case a complex tri-axial stress tensor is studied.

3.1 Bar element formulation

3.1.1 Linear 1D CM formulation

The CM requires the definition of two cell complexes, usually referred to as primal and dual, linked by duality relations. If N is the dimensionality of the manifold, duality implies a one-to-one correspondence between a generic primal p -geometrical entity (node, edge, face or volume) and the correspondent dual $N - p$ one (volume, face, edge, node, respectively). Each physical variable is univocally associated to an oriented spatial element. When global variables are used (e.g. integration of pointwise quantities on the spatial element they are related to), this geometric set up allows the use of discrete operators which are representative of the continuous gradient, curl and divergence. It is easy to prove that these discrete operators are the incidence matrices \mathbf{G} (edge-to-node), \mathbf{C} (face-to-edge), \mathbf{D} (volume-to-face) made of 0, 1, -1 . Geometric duality is required to maintain the duality relation between primal and dual topological operators [Tonti (2002)]. As far as the elastostatics is concerned, duality requires that:

$$\tilde{\mathbf{D}} = -\mathbf{G}^T \tag{11}$$

where the $\tilde{\cdot}$ indicates that the incidence matrix is constructed on the dual mesh. Material operators are represented by square matrices \mathbf{M} that link together quantities associated to dual pairs of cell complexes. In the case of the elastostatics such operator links the difference of displacements with surface forces. The stiffness matrix representing the discretized version of the continuous problem can be assembled by the product of topological and constitutive matrices:

$$\mathbf{K} = \tilde{\mathbf{D}}\mathbf{M}\mathbf{G} = -\mathbf{G}^T\mathbf{M}\mathbf{G} \tag{12}$$

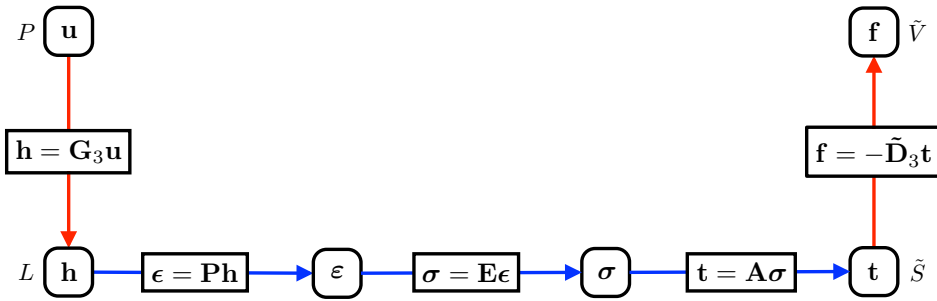


Figure 1: Tonti Diagram of the elastostatic problem.

Table 1: Global variables used in the CM formulation and their assignment to spatial elements.

cell complex	variable	symbol	spatial entity
primal	displacement	u	node
	displacement difference	h	edge
dual	surface force	t	face
	volume force	f	volume

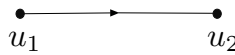


Figure 2: Elementary 1D primal discretization with orientation.

These concepts are summarized in the so-called Tonti diagrams, as shown in Fig. 1. The variables involved in the CM formulation of elastostatics are summarized in Tab. 1

Considering for simplicity a 1D bar element as shown in Fig. 2, the displacement difference can be written as:

$$h = u_2 - u_1 = \begin{bmatrix} -1 & 1 \end{bmatrix} \begin{bmatrix} u_1 \\ u_2 \end{bmatrix} \tag{13}$$

The surface forces, acting on dual faces, Fig. 3, are part of the balance equation through the discrete divergence $\tilde{\mathbf{D}}$ [Tonti (2001); Cosmi (2001, 2005); Tonti and Zarantonello (2009)]

$$-\begin{bmatrix} 1 \\ -1 \end{bmatrix} t = \begin{bmatrix} f_1 \\ f_2 \end{bmatrix} \tag{14}$$

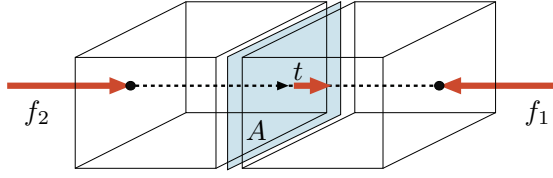


Figure 3: Forces acting on dual columes.

The point wise constitutive equation of elastostatics links stresses and strains:

$$\sigma = E\varepsilon \tag{15}$$

Within the CM, the constitutive equation is formulated by relating the variation of displacement with the surface forces. To this aim, stresses and strains must be related to surface forces and displacement differences, respectively (for implementation detail see [Alotto, Freschi, Repetto, and Rosso (2013)]):

$$t = A\sigma \tag{16}$$

$$\varepsilon = \frac{1}{L}h \tag{17}$$

By combining all the above-mentioned equations it is possible to write the final equation that solves the elastic problem:

$$-\begin{bmatrix} 1 \\ -1 \end{bmatrix} AE \frac{1}{L} \begin{bmatrix} -1 & 1 \end{bmatrix} \begin{bmatrix} u_1 \\ u_2 \end{bmatrix} = E \frac{A}{L} \begin{bmatrix} 1 & -1 \\ -1 & 1 \end{bmatrix} \begin{bmatrix} u_1 \\ u_2 \end{bmatrix} = \begin{bmatrix} f_1 \\ f_2 \end{bmatrix} \tag{18}$$

When the problem is discretized by many 1D elements, it is easy to re-formulate the problem in matrix form. Eq. (13) to Eq. (16) become:

$$\mathbf{h} = \mathbf{G}\mathbf{u} \tag{19}$$

$$-\tilde{\mathbf{D}}\mathbf{t} = \mathbf{f} \tag{20}$$

$$\sigma = \mathbf{E}\varepsilon \tag{21}$$

$$\mathbf{t} = \mathbf{A}\sigma \tag{22}$$

$$\varepsilon = \mathbf{L}^{-1}\mathbf{h} = \mathbf{P}\mathbf{h} \tag{23}$$

Finally the solve equation for elastostatics reads

$$-\tilde{\mathbf{D}}\mathbf{A}\mathbf{E}\mathbf{P}\mathbf{G}\mathbf{u} = \mathbf{f} \tag{24}$$

By using the duality Eq. (11), and assembling the constitutive matrix as $\mathbf{M}_E = \mathbf{AEP}$

$$\tilde{\mathbf{G}}^T \mathbf{M}_E \mathbf{G}\mathbf{u} = \mathbf{f} \tag{25}$$

3.1.2 Nonlinear 1D formulation

The nonlinearity that is relevant for the present discussion is inherent in the elastoplastic behavior of the material; therefore the fixed point method will be applied to the nonlinear relationship between stresses and strains. Therefore, considering that the total deformation can be divided into two components, elastic deformation and plastic deformation, the elastic behavior can be described with the classical relationship $\sigma = E\varepsilon$ while the plastic behavior can be described by the Ramberg-Osgood law:

$$\sigma = \sigma_0 + K_{RO} \cdot \varepsilon_p^m \quad (26)$$

where σ_0 represents the yield point of the material. Considering a single point in which it is possible to determine the strain, it is possible to calculate the corresponding stress, by means of the two laws above described.

The fixed point method is applied using as linearization coefficient of the nonlinear curve the initial slope E of the material characteristic, which is a value that guarantees the convergence. Using this value for each cell of the discretized domain the stiffness matrix is computed. The iterative process is summarized in Fig. 4, where the functionality of the method is depicted.

The nonlinear iterative scheme, highlighted in the flow-chart of Fig. 5, starts solving the elastostatic problem for the first step, as expressed in Eq. (25), using a stiffness matrix estimated on the basis of the Young modulus. Then, the strains are computed from the displacement differences:

$$\boldsymbol{\varepsilon} = \mathbf{P}\mathbf{G}\mathbf{u} \quad (27)$$

For each cell, the strain is used as the abscissa of the stress-strain curve. In this way it is possible to estimate a stress, named σ_p , on the curve of the material and a stress σ_{fp} obtained on the line that depicts the linearization of the stiffness matrix. The difference between the two estimated stresses ($\sigma_{fp} - \sigma_p$) represents the residue as defined in Eq. (9). The residual stress should be converted in a residual force, in order to add this residual force vector to the external forces \mathbf{f} . The advantage of this technique is therefore to determine a unique stiffness matrix for the whole nonlinear process, factorizing only once and re-using the factorization at each iteration. This approach allows a reduction in the computational effort but, on the other hand, its convergence is usually slower compared to the case of the Newton-Raphson technique.

3.2 Nonlinear 3D formulation

In analogy with the 1D formulation, also the implementation of the technique for a three-dimensional tetrahedral element is performed. In this case it is necessary

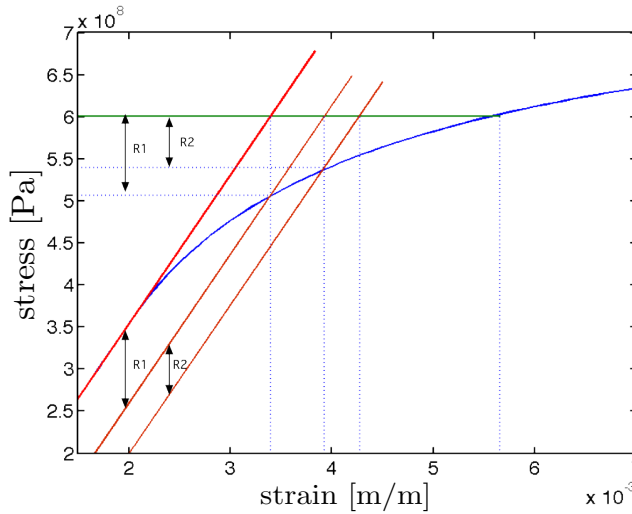


Figure 4: Fixed Point method applied to the stress-strain curve. The blue curve describes the nonlinear characteristic of the material and allows to calculate σ_p , the red line depicts the linear law used to calculate the stress σ_{fp} .

to develop a criterion to compute the value of the forces produced by the residuals calculated at each iteration, starting from the strain and stress tensors of each individual element. Details about the 3D CM formulation can be found in [Alotto, Freschi, Repetto, and Rosso (2013)].

It is important to underline that in the CM formulation, strains and stresses are assumed uniform within the element. The stress and strain tensors should be related each other by means of the material features and to this purpose, a multi-axial criterion should be adopted. In order to pass from the triaxial stress and strain state to an equivalent scalar, the Von Mises criterion is used. This equivalent state is useful for computing the residual stress, but this quantity should be then transformed in a residual force. A reverse process should be then adopted to extend the calculated residue (that is a one-dimensional value) in three dimensions, with the aim to obtain a force value for each direction and for each node. The assumption behind the von Mises criterion is that the principal directions of stress and strain remain parallel to each other and thereby it is possible to define a scale factor between the main directions of stress and strain. Once the stress and strain tensors for each element using the three-dimensional linearized model [Alotto, Freschi, Repetto, and Rosso (2013)] are calculated, the main stress and strain directions should be computed, and then applying the von Mises criterion to evaluate the equivalent strain,

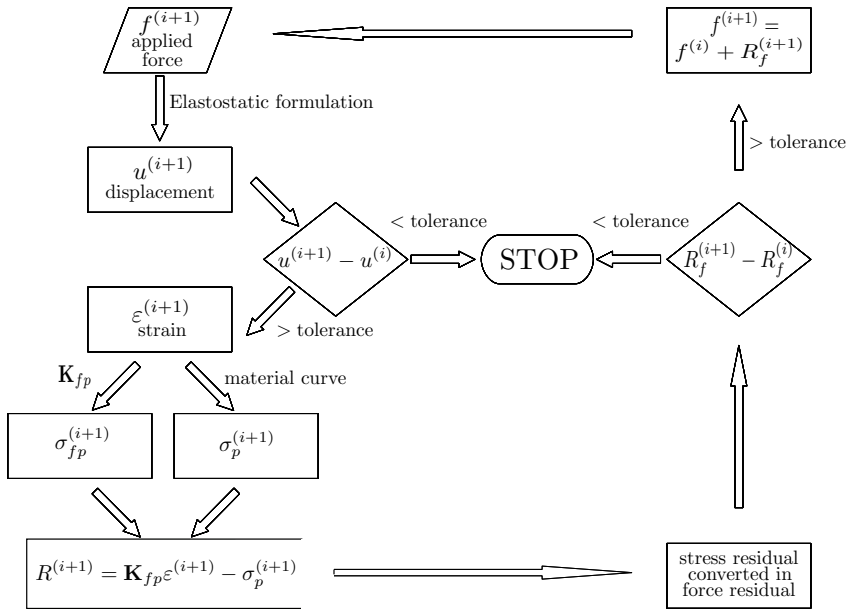


Figure 5: Flow-chart for the determination of the displacement in the nonlinear bar element.

the equivalent stress can be evaluated on the material curve. Using the equivalent stress and the main stresses, a weighting factor α can be determined for each main direction and the residual force can be projected along them:

$$\alpha_1 = \frac{\sigma_1}{\sigma_{VM}}; \quad \alpha_2 = \frac{\sigma_2}{\sigma_{VM}}; \quad \alpha_3 = \frac{\sigma_3}{\sigma_{VM}} \quad (28)$$

Therefore, by using the nonlinear stress and the fixed point stress, the residual stress can be computed. By using the coefficients calculated in Eq. (28) and the principal directions, the residual stress is projected in a stress tensor. As in the previous case the residual force is computed and it can be added to the external loads in order to start the iterative process. In Fig. 6, the algorithm is sketched; the residual force thus assumes a physical meaning of force which is added to the linear case in order to compensate the nonlinearity of the material.

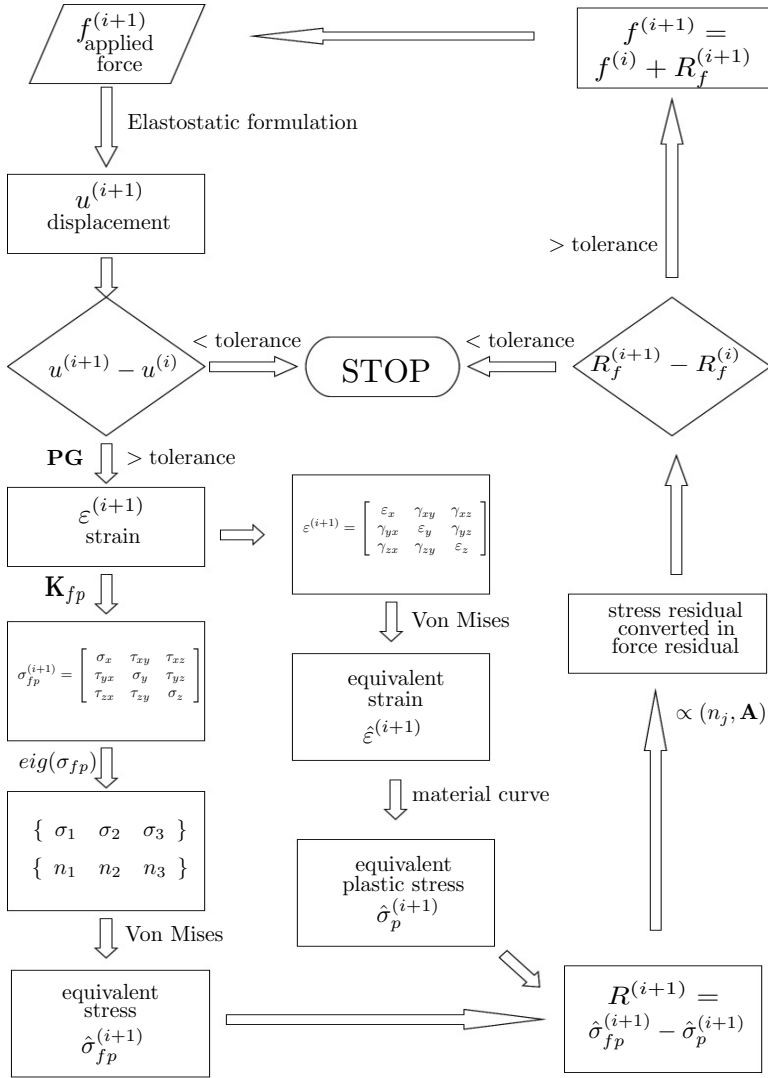


Figure 6: Flow-chart for determining the displacement in the three-dimensional nonlinear element.

4 Validation of the proposed procedure

4.1 Test case for the nonlinear one-dimensional bar element formulation

In order to validate the procedure a $L = 50$ mm ($a = 30$ mm, $b = 20$ mm), steel bar is considered. Fig. 7 shows the geometry and the 1D discretization. The bar is

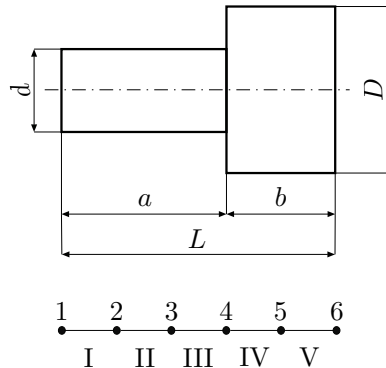


Figure 7: Geometry and model of the bar used to validate the proposed procedure.

constrained at one end and subjected to a tensile force $F = 40$ kN at the opposite extreme. It presents two cross sections ($d = 12.5$ mm, $D = 17.7$ mm) designed to generate a stress state beyond the yield limit in the lower section portion, while in the other section the tensile stress does not exceed the yield strength of the material. The mechanical behavior is described as $\sigma = \sigma_0 + K_{RO}\epsilon_p^m = 290 + 610 \cdot \epsilon_p^{0.56}$, where the yield stress is equal to 290 MPa. In Tab. 2 the displacements and the strains computed by the proposed model are summarized with respect to the initial and final iterations and compared with the analytical values computed using the material curve. The analytical values are computed with the following process:

- the stresses in the sections are computed using the external force and the areas of the two sections;
- then, the corresponding strains are evaluated using the material characteristic curve and the computed stresses;
- finally, the strains are multiplied by the section lengths and the final displacements are computed.

The value of the strain remains constant in the two elements that do not reach plasticization, while in the three plasticized elements the strain varies within the iteration process until it reaches a value at which the errors are below a tolerance equal to 10^{-8} .

4.2 Test cases for the nonlinear three-dimensional formulation

The 3D nonlinear iterative technique is numerically compared versus a commercial software and with respect to experimental data.

Table 2: Computed values of node displacement and element strain in the iterative process.

	geometric entity	Initial value	Final value	Analytical value
displ. (10^{-4} m)	node 1	0	0	0
	node 2	0.155	0.729	0.729
	node 3	0.310	1.458	1.458
	node 4	0.466	2.188	2.188
	node 5	0.543	2.265	2.265
	node 6	0.621	2.343	2.343
strain (10^{-3} $\frac{m}{m}$)	element I	1.55	7.29	7.30
	element II	1.55	7.29	7.30
	element III	1.55	7.29	7.30
	element IV	0.77	0.77	0.77
	element V	0.77	0.77	0.77

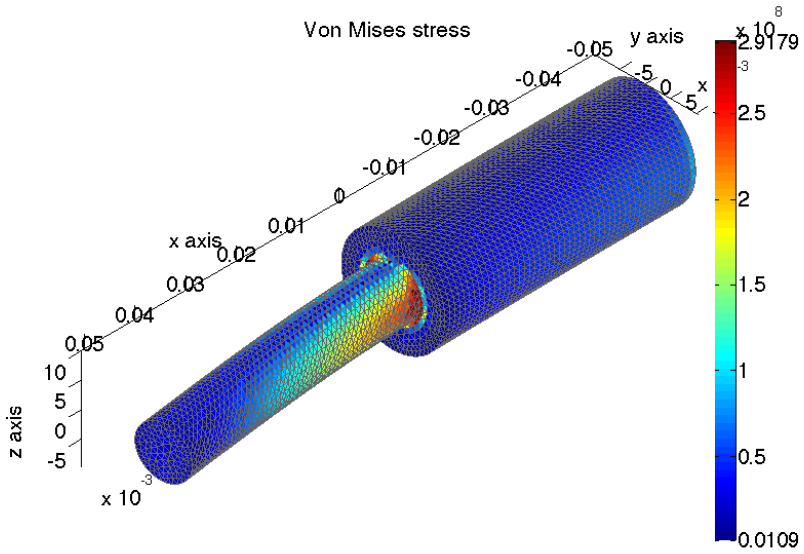
4.2.1 Comparison with FE analysis

The numerical comparison is performed on a simple a cylindrical bar of 100 mm length with two different sections, for half of its length with a diameter $d_1 = 10$ mm and for the second half with a diameter $d_2 = 20$ mm. The bar is fixed at the larger end, whereas on the other end it is loaded with a shear force of 590 N that creates a bending moment. The benchmark is solved with the DualLab code [Freschi, Giaccone, and Repetto (2008)], a Matlab Toolbox that implements the cell method, and with the commercial FE software Abaqus 6.10. Both in CM and FE analysis share the same mesh, made of 1767 nodes and 7791 tetrahedra. The results are obtained with a tolerance of the nonlinear iterations on displacement equal to 10^{-8} .

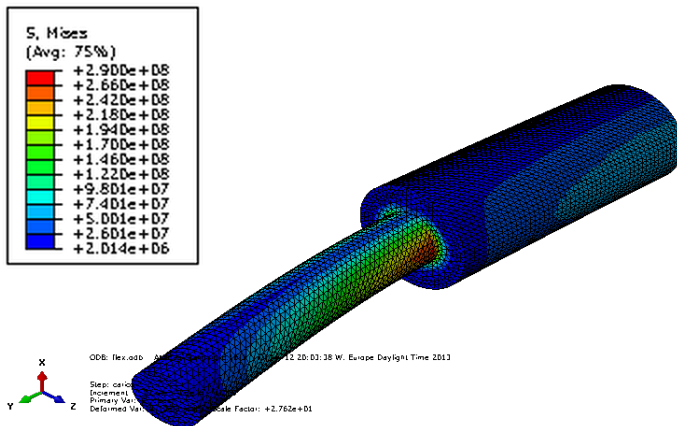
Fig. 9 shows the comparison between the displacements calculated with the CM and FE. With reference to the maximum displacement of the bar, the CM estimates a value of 3.64×10^{-4} m, while Abaqus calculates a displacement of 3.62×10^{-4} mm Fig. 8 shows the colormaps of Von Mises stresses calculated via the CM and FE. The maximum stress calculated with the CM is 292 MPa, while Abaqus returns a value of 290 MPa. In both analysis, the relative difference between the two methods is lower than 1 %, proving the accuracy of the method.

4.2.2 Comparison with experimental results

The comparison with an actual test case is conducted using a specimen subject to bending on three points as shown in Fig. 10. The characteristics of the speci-

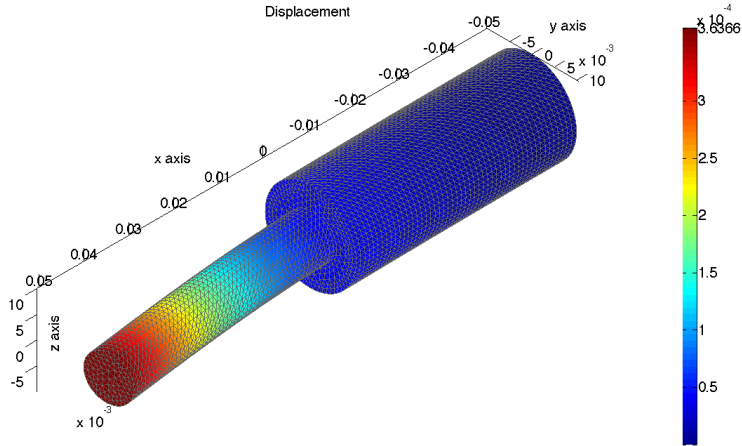


(a) Cell method (DualLab)

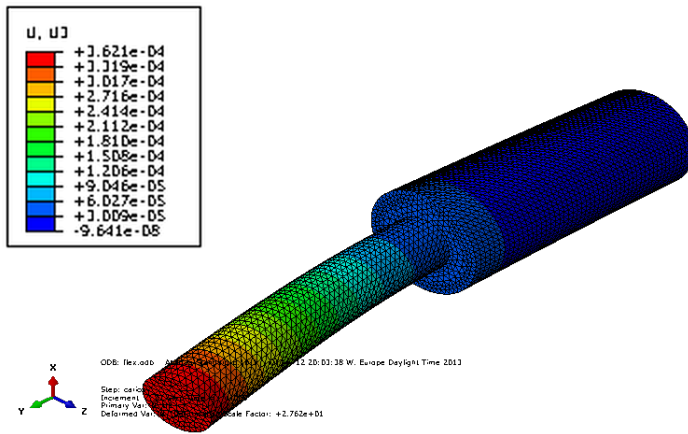


(b) Finite element (Abaqus)

Figure 8: Color map visualization of Von Mises stresses.



(a) Cell method (DualLab)



(b) Finite element (Abaqus)

Figure 9: Color map visualization of displacements.

Table 3: Comparison between measured and computed displacements.

Force (N)	Displacements (mm)	
	Measured	Computed by CM
50	0.023	0.023
1000	0.460	0.453
3000	1.568	1.509
4000	2.255	2.423

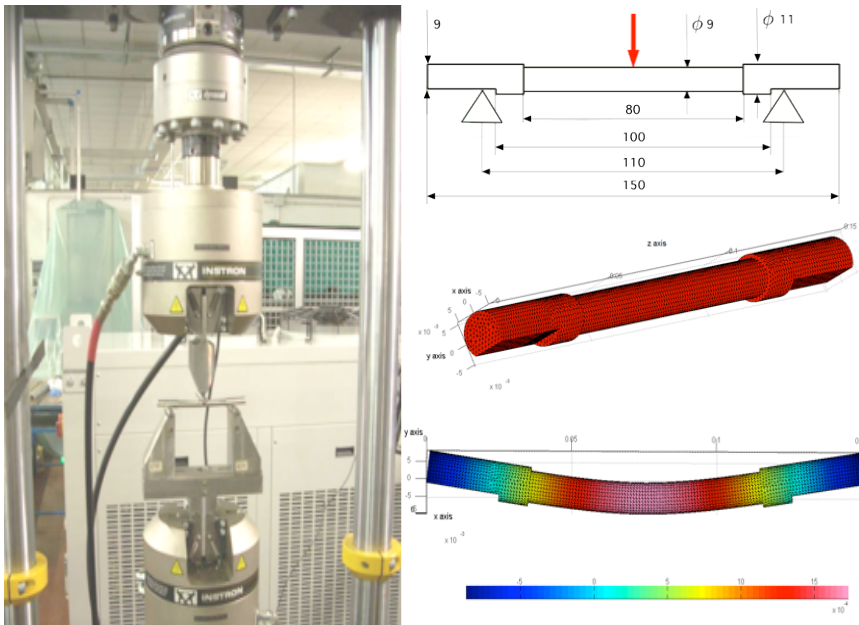


Figure 10: Experimental test and corresponding modelling.

men material are known through a tensile test campaign conducted by the authors to evaluate the experimental relationship between stress and strain. The specimen has a maximum external diameter of 10 mm and it is made to reach plastic deformation in the middle of its span; the geometry presents two little flattenings in order to obtain an easy fit on the fixed supports. During the experimental test the curve force-crosshead displacement is recorded and the process is then numerically modeled in DualLab. The material features are implemented as a look-up table in DualLab code in order to follow the material law. Boundary conditions are defined as simply supported conditions and the loading force is applied on a little area in

the middle of the model span. The model is made by 13194 nodes and 64417 tetrahedra. It is subject to different load conditions and the relative tolerance on the displacements for the convergence of the nonlinear iterations is set to 10^{-8} . The obtained results are summarized in Tab. 3; the deviation between the experimental and the numerical results (less than 4% in any case) could be ascribed to the compliance of the support devices of the specimen in the actual test system, while the model has not deformable constraints.

5 Analysis of a commercial automotive exhaust manifold

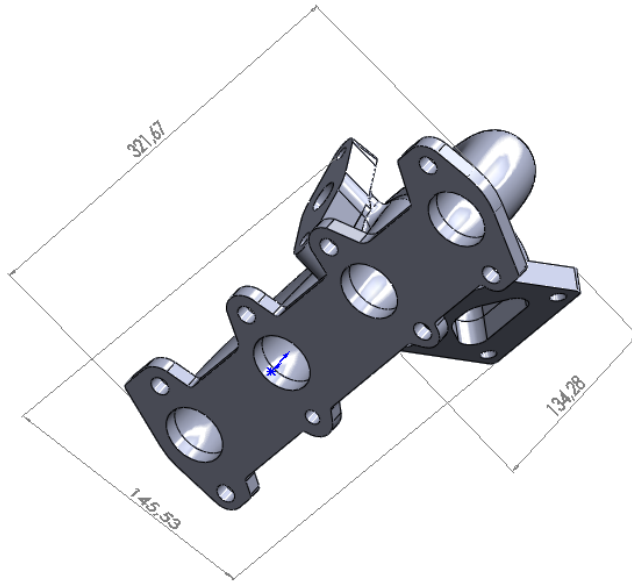
In order to test the procedure on an actual application, a multiphysics example is studied. Using the same model described in [Alotto, Freschi, Repetto, and Rosso (2013); Delprete, Rosso, and Vercelli (2010)] and introducing the material properties in terms of strain vs stress and temperature, the computation of four heating cycles is then performed and the obtained results are analyzed.

5.1 Model description

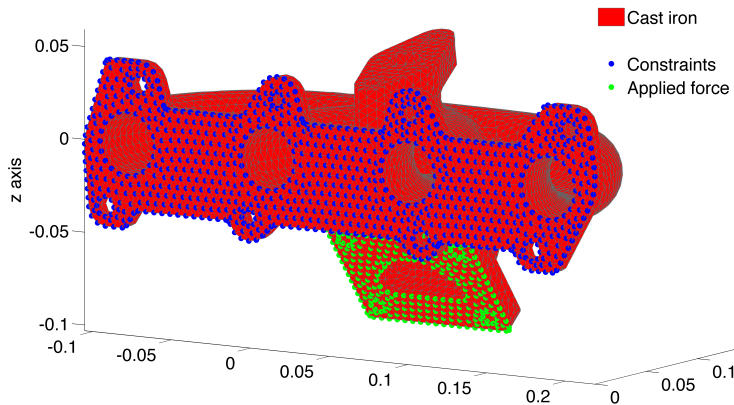
The model has a 3D mesh of first order four-node tetrahedral elements generated by means of a commercial pre-processing code; the total number of nodes is 13567, while 45990 are the solid elements (for complete model information and details see [Alotto, Freschi, Repetto, and Rosso (2013); Delprete, Rosso, and Vercelli (2010)]). The thermal part of the model is the same of [Delprete, Rosso, and Vercelli (2010)] and the variation of the material properties with temperature is reported in Tab. 4. The boundary conditions are represented by a fully locked flange (the most severe analysis condition, not corresponding to the actual application, but useful to understand the quality of the overall exhaust manifold design) and by the application of a constant mass to simulate the turbo unit (4 kg). The exhaust gas temperature variation in the ducts and the heat conduction condition on the external surfaces of the exhaust manifold complete the time variant boundary conditions. In Fig. 11(a) a sketch of the model is shown and the corresponding DualLab model is presented in Fig. 11(b). In Fig. 12 the four heating cycles imposed as thermal boundary conditions are shown.

5.2 Nonlinear behavior of the material

The most important nonlinearities in this model are concentrated in the material behavior. The material changes its features with respect to the temperature and the increment of strain, so different curves are needed to describe the material. In order to extract those curves, experimental tests on specimens of the same cast iron the manifold is made of are conducted by the authors and the material parameters are



(a) Main dimensions (in mm)



(b) Discretization and mechanical boundary conditions

Figure 11: Exhaust manifold model.

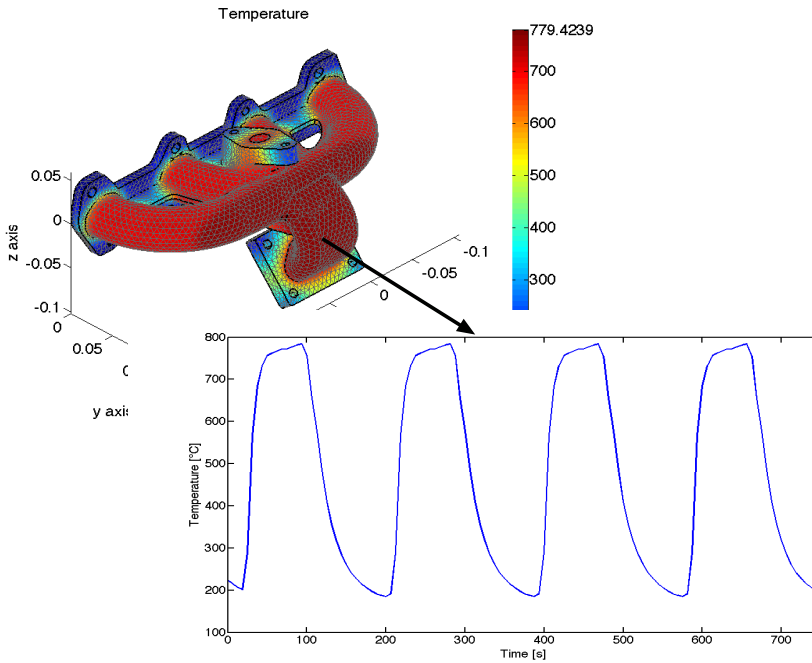


Figure 12: Temperature trend [Delprete, Rosso, and Vercelli (2010)] imposed to the numerical model as thermal boundary condition; in particular the trend is associated to the warmer zone of the manifold model.

Table 4: Material (Si-Mo-Cr cast iron, [Delprete, Rosso, and Vercelli (2010)]) parameters at different temperature.

Characteristic	SI units	Temperature		
		20 °C	400 °C	700 °C
Young modulus	Pa	1.768×10^{11}	1.483×10^{11}	0.84×10^{11}
Poisson ratio	-	0.26	0.26	0.26
Density	kg/m ³	7100	7100	7100
Thermal expansion	K ⁻¹	1.14×10^{-5}	1.21×10^{-5}	1.33×10^{-5}
Thermal conduction	W/(m ² K)	25.1	30	29
Heat capacity	J/(kgK)	607	607	607
Yield stress σ_0	Pa	338.592×10^6	209.191×10^6	101.333×10^6
Yield constant K_{RO}	Pa	7×10^8	3.3×10^8	1.5×10^8
Plastic exponent m	-	0.12	0.048	0.135

figured out; at present the paper reporting the material parameters is under editing process. In Tab. 4 the parameters used to define the material behavior are reported. In order to take into account the presence of the elastic strain before the plastic zone, the Ramberg-Osgood law Eq. (26) should be modified in:

$$\sigma = \sigma_0 + K_{RO}\varepsilon^m - K_{RO} \frac{(\sigma_0/E)^{m+1}}{\varepsilon} \tag{29}$$

So it is possible to divide the material behavior in two regions: one where strains are lower than the yield strain, that is represented by a linear relationship, and a second region where the Ramberg-Osgood law works, that depicts the plastic behavior of the material. This procedure is applied for three temperatures, as shown in Fig. 13.

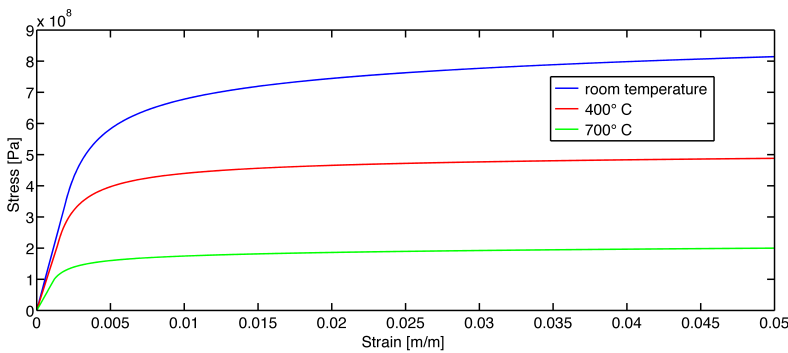


Figure 13: Material characteristics computed at three different temperatures by using data of Tab. 4 and Eq. (29).

5.3 Computational scheme for the solution of the coupled problem

The implemented solution scheme starts with the solution of the combined thermal and linear elastic problem for each time instant. The elastic and thermal constitutive matrices are estimated on the basis of the temperature computed at the previous step.

A note has to be underlined: temperature is a configuration variable whereas stress is a source variable, so the material characteristics are defined in the center of gravity of the cell and a rule for evaluating the temperature in the dual cell should be defined. The implemented approach computes the cell temperature as the mean of the nodal temperatures. Then, by knowing the cell temperature, the material features are selected, so the cell stiffness is defined and each thermal force is computed (for detail see [Alotto, Freschi, Repetto, and Rosso (2013); Delprete, Rosso, and

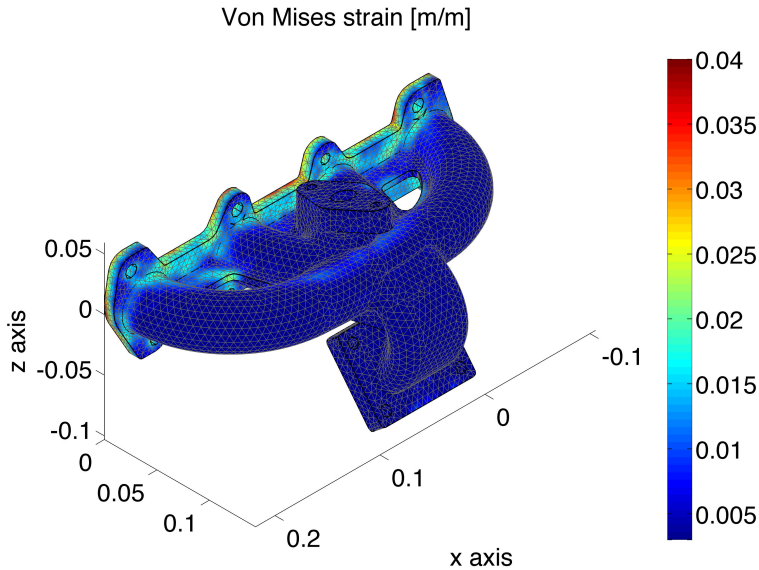


Figure 14: Exhaust manifold strains computed after four thermal cycles.

Vercelli (2010)). In each time instant, after the first computation of temperatures and displacements, the nonlinear procedure starts following the flow-chart reported in Fig. 6. When the convergence of the fixed point method is found, the solution procedure passes to the next time instant and the solution goes on until the final time instant.

5.4 Computed results

In Fig. 14 the colormap of the exhaust manifold strains after four thermal cycles is reported; it is comparable with that usually computed in the industrial practice using FE procedures (for example see [Watanabe, Shiratani, Iwanaga, and Nishino (1998); Hazime, Dropps, Anderson, and Ali (2003); Fan, Kuba, and Nakanishi (2004)]). The maximum value of strain of about 0.04 m/m is reached because no rupture conditions are specified in the model and the constraints are more rigid than the actual ones. The same consideration can be highlighted in terms of stresses as reported in Fig. 15, where the maximum value of stress after four thermal cycles is about of 800 MPa compatible with the stress/strain behavior of the material at room temperature (that is the final temperature of the heating process).

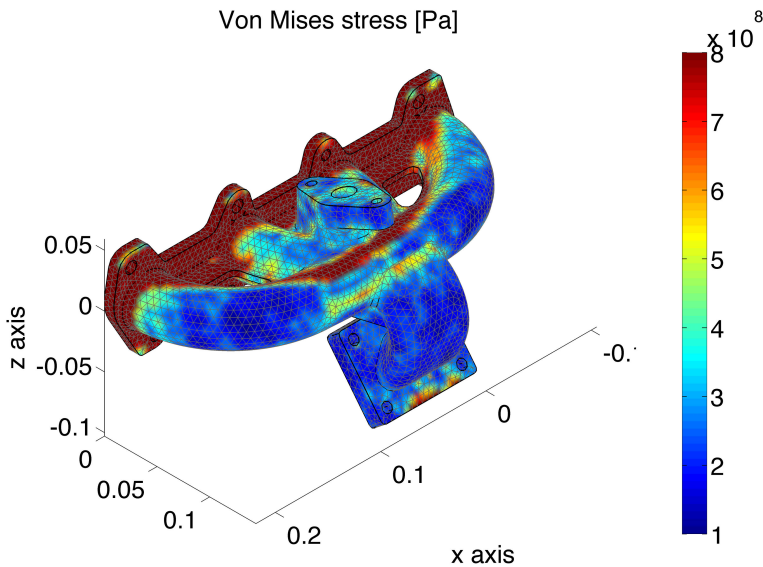


Figure 15: Exhaust manifold stresses computed after four thermal cycles.

6 Conclusions

On the basis of the shown results, it can be stated that the proposed procedure is able to analyze with adequate precision nonlinear problems in the mechanical structural field.

The advantage of the presented technique is to allow a truly multiphysics approach to engineering problems and the introduction of a nonlinear solver able to deal with all the nonlinearities present in physical coupled problems, opens very interesting scenarios of future research works.

As also presented in [Delprete, Freschi, Repetto, and Rosso (2009); Delprete, Rosso, and Vercelli (2010)], thermo-structural investigations of mechanical components appear to be optimal candidates for the application of the procedure here proposed. The necessary step for the analysis of an actual component is the introduction of a policy that cumulates plasticity and permits the recognition of the breaking point of the material, at the moment not yet covered by the proposed technique and that will represent a future development of the research.

References

- Alotto, P.; Freschi, F.; Repetto, M.** (2010): Multiphysics problems via the cell method: The role of tonti diagrams. *IEEE Transactions on Magnetics*, vol. 46, no. 8, pp. 2959–2962.
- Alotto, P.; Freschi, F.; Repetto, M.; Rosso, C.** (2013): *The Cell Method for Electrical Engineering and Multiphysics Problems, An Introduction*. Springer Verlag, Berlin-Heidelberg.
- Chiampi, M.; Chiarabaglio, D.; Repetto, M.** (1994): An accurate investigation on numerical methods for nonlinear magnetic field problems. *Journal of Magnetism and Magnetic Materials*, vol. 133, pp. 591–595.
- Constantinescu, A.; Charkaluk, E.; Lederer, G.; Verger, L.** (2004): A computational approach to thermomechanical fatigue. *International Journal of Fatigue*, vol. 26, pp. 805–818.
- Cosmi, F.** (2001): Numerical solution of plane elasticity problems with the cell method. *Computer Modeling in Engineering & Science*, vol. 2, no. 3, pp. 365–372.
- Cosmi, F.** (2005): Elastodynamics with the cell method. *Computer Modeling in Engineering & Sciences*, vol. 8, no. 3, pp. 191–200.
- Delprete, C.; Freschi, F.; Repetto, M.; Rosso, C.** (2009): Thermo-mechanical analysis using a multiphysics approach. *Journal of Physics: Conference Series*, no. 181.
- Delprete, C.; Freschi, F.; Repetto, M.; Rosso, C.** (2010): Experimental validation of a numerical multiphysics technique for electro-thermo-mechanical problem. *The International Journal for Computation and Mathematics in Electrical and Electronic Engineering*, vol. 29, no. 6, pp. 1642 – 1652.
- Delprete, C.; Rosso, C.** (2005): Exhaust manifold thermo-structural simulation methodology. *SAE Technical Paper Series*, , no. 2005-01-1076.
- Delprete, C.; Rosso, C.; Vercelli, A.** (2010): Thermo-mechanical analysis of a cast iron exhaust manifold: a comparison between the traditional and a new methodology. *SAE Technical Paper Series*, , no. 2010-01-0498.
- Fan, Q. Y.; Kuba, M.; Nakanishi, J.** (2004): Coupled analysis of thermal flow and thermal stress of an engine exhaust manifold. *SAE Technical Paper*, vol. 2004-01-1345.
- Ferretti, E.** (2013): The cell method: an enriched description of physics starting from the algebraic formulation. *CMC: Computers, Materials and Continua*, vol. 36, no. 1, pp. 49 – 72.

Ferretti, E. (2013): A cell method stress analysis in thin floor tiles subjected to temperature variation. *CMC: Computers, Materials and Continua*, vol. 36, no. 3, pp. 293 – 392.

Freschi, F.; Giaccone, L.; Repetto, M. (2008): Educational value of the algebraic numerical methods in electromagnetism. *COMPEL - The International Journal for Computation and Mathematics in Electrical and Electronic Engineering*, vol. 27, no. 6, pp. 1343–1357.

Hazime, R. M.; Dropps, S. H.; Anderson, D. H.; Ali, M. Y. (2003): Transient non-linear FEA and TMF life estimates of cast exhaust manifolds. *SAE Technical Paper*, vol. 2003-01-0918.

Mamiya, N.; Masuda, T.; Noda, Y. (2002): Thermal fatigue life of exhaust manifolds predicted by simulation. *SAE Technical Paper*, vol. 2002-01-0854.

Moro, E.; Alotto, P.; Freschi, F.; Guarnieri, M. (2012): A cell method formulation of 3-D electrothermomechanical contact problems with mortar discretization. *IEEE Transactions on Magnetics*, vol. 42, no. 2, pp. 503–506.

Su, X.; Zubeck, M.; Lasecki, J., Jr., E.-P.; Tang, C.; Sehitoglu, H.; Allison, J. (2002): Thermal fatigue analysis of cast aluminium cylinder heads. *SAE Technical Paper Series*, , no. 2002-01-0657.

Tonti, E. (2001): A direct discrete formulation of field laws: The cell method. *Computer Modeling in Engineering & Sciences*, vol. 2, no. 2, pp. 237–258.

Tonti, E. (2002): Finite Formulation of Electromagnetic Field. *IEEE Transactions on Magnetics*, vol. 38, pp. 333–336.

Tonti, E.; Zarantonello, F. (2009): Algebraic formulation of elastostatics: the cell method. *Computer Modeling in Engineering & Sciences*, vol. 39, no. 3, pp. 201 – 236.

Watanabe, Y.; Shiratani, K.; Iwanaga, S.; Nishino, K. (1998): Thermal fatigue life prediction for stainless steel exhaust manifold. *SAE Technical Paper*, vol. 980841.

Wohrmann, R.; Seifert, T.; Willeke, W.; Hartmann, D. (2006): Fatigue life simulation for optimized exhaust manifold geometry. *SAE Technical Paper*, vol. 2006-01-1249.

Zienkiewicz, O.; Taylor, R. (2000): *The Finite Element Method - Volume 1: The Basis*. Butterworth-Heinemann, fifth edition.